EVALUATION OF THE SHAW MODEL IN SIMULATING THE COMPONENTS OF NET ALL-WAVE RADIATION

W. Xiao, G. N. Flerchinger, Q. Yu, Y. F. Zheng

ABSTRACT. *Radiation exchange at the surface plays a critical role in the surface energy balance, plant microclimate, and plant growth. The ability to simulate the surface energy balance and the microclimate within the plant canopy is contingent upon accurate simulation of the surface radiation exchange. A validation exercise was conducted of the Simultaneous Heat and Water (SHAW) model for simulating the surface radiation exchange (including downward long-wave and upward short- and long-wave radiation) over a maize canopy surface using data collected at Yucheng in the North China Plain. The model simulated upward short-wave and net all-wave radiation well with model efficiencies (ME) equaling 0.97 and 0.98, respectively. Downward and upward long-wave radiation were overestimated by 12.1 and 8.3 W m^{-2} with ME equaling 0.68 and 0.89, respectively. Two modifications to the model were implemented and tested to improve the simulated long-wave radiation exchange. In one modification, alternative schemes were tested to simulate cloudy sky long-wave radiation, and the best algorithm was employed in the model. With this modification, both downward and upward long-wave radiation were simulated better, with ME rising to 0.88 and 0.91, respectively. A second modification was implemented to use leaf temperature rather than canopy air temperature to compute emitted long-wave radiation. Although more theoretically correct, this modification did not improve simulations compared to the original model because upward long-wave radiation was already overpredicted and midday leaf temperatures at this site were typically higher than canopy air temperatures. Thus, the modification resulted in even higher overprediction of upward midday long-wave radiation. However, this modification removed some of the bias in nighttime emitted long-wave radiation. While the SHAW model simulates the radiation balance and transfer processes within the canopy reasonably well, results point to areas for model improvement.*

Keywords. *Long-wave radiation, Maize canopy, Short-wave radiation, Surface energy balance.*

All surfaces receive short-wave radiation during daylight and exchange long-wave radiation continuously with the atmosphere. This exchange is the driving force for the surface energy balance, influences canopy skin temperature, and provides the energy for photosynthesis and plant growth. Accurate simulations of canopy microclimate, its influence on plant processes, and water and CO_2 exchange are contingent on simulation of the surface radiation balance.

The net amount of radiation received by a surface is defined by the equation:

$$R_n = S_d - S_u + L_d - L_u \tag{1}$$

where R_n is net all-wave radiation, S_d is downward short-wave solar radiation incident on the surface, S_u is short-wave radiation reflected by the surface to the sky, L_d is downward long-wave radiation emitted from the atmosphere, and L_u is long-wave radiation emitted from the surface to the atmosphere. Measurements of S_d are typically input to simulation models. Several parameterizations have been developed that produce estimates for L_d using synoptic observations (e.g., Idso and Jackson, 1969; Maykut and Church, 1973; Jacobs, 1978; Idso, 1981; Aubinet, 1994; Dilley and O'Brien, 1998). Estimations of the upward fluxes from the surface (S_u and L_u) differ widely between simulation models depending on whether they are single-source (Monteith, 1963), dual-source (Shuttleworth and Wallace, 1985; Huntingford et al., 1995), or multiple-source models (Norman, 1979; Smith and Goltz, 1994; Flerchinger et al., 1998; Zhao and Qualls, 2005). Multiple-source models are required to model radiation distribution and microclimate profiles throughout the canopy.

The Simultaneous Heat and Water (SHAW) model originally developed by Flerchinger and Saxton (1989) was modified by Flerchinger and Pierson (1991) to simulate microclimate conditions within a plant canopy. The SHAW model's ability to simulate heat, water, and chemical movement through plant cover, snow, residue, and soil for predicting climate and management effects on soil freezing and thawing (Flerchinger and Hanson, 1989; Hayhoe, 1994), frost (Kennedy and Sharratt, 1998; Flerchinger and Seyfried, 1997), snowmelt (Flerchinger et al., 1994; Duffin, 1999), soil temperature, soil water (Flerchinger and Pierson, 1991;

Submitted for review in November 2005 as manuscript number SW 6145; approved for publication by the Soil & Water Division of ASABE in July 2006.

The authors are **Wei Xiao,** Graduate Student, Institute of Geographical Sciences and Natural Resources Research, Chinese Academy of Sciences, and Graduate School of the Chinese Academy of Sciences, Beijing, China; **Gerald N. Flerchinger, ASABE Member Engineer,** Research Hydraulic Engineer, USDA-ARS Northwest Watershed Research Center, Boise, Idaho; **Qiang Yu,** Professor, Institute of Geographical Sciences and Natural Resources Research, Chinese Academy of Sciences, Beijing, China; and **You Fei Zheng,** Professor, Department of Environmental Sciences, Nanjing University of Information Science and Technology, Nanjing, China. **Corresponding author:** Qiang Yu, Institute of Geographical Sciences and Natural Resources Research, Chinese Academy of Sciences, No. 11 Datun Road, Beijing 100101, China; phone: 86-10-64856515; fax: 86-10-64851844; e-mail: yuq@igsnrr.ac.cn.

Hymer et al., 2000; Xu et al., 1991), evaporation, transpiration, energy flux (Flerchinger et al., 1996a, 1996b; Nassar et al., 2000), and surface temperature (Flerchinger et al., 1998) has been demonstrated, as well as its ability to simulate the effects of residue type and architecture on heat and water transfer in significantly different climates (Flerchinger et al., 2003).

Xiao et al. (2006) evaluated the SHAW model's ability to simulate the surface energy balance and temperature and water vapor profiles within a plant canopy and identified weaknesses in the model for simulating the canopy microclimate. Detailed validation of all components of the radiation exchange simulated by the SHAW model has never been conducted. In light of results obtained by Xiao et al. (2006), such a validation is warranted to ensure that the radiation exchange driving mircrometeorological processes is accurately simulated prior to further within-canopy assessment of the canopy routines. Therefore, the objectives of this research were to: (1) validate the surface radiation balance simulation of the SHAW model over a well-irrigated maize canopy using data collected at Yucheng in the North China Plain, and (2) evaluate modifications to the model to improve predictions of long-wave radiation exchange.

Methods

The field experiment was conducted at the Yucheng Comprehensive Experiment Station (36° 50' N, 116° 34' E, 28 m a.s.l.) of the Chinese Academy of Sciences, lying on the North China Plain (NCP). Measurements were made at the center of a 300 × 300 m, well-watered field of maize. Surrounding the experimental field were unbroken fields of maize, at similar growth stages and available water supply, extending at least 5 km in all directions.

Micrometeorological variables such as air temperature, wind speed, and relative humidity were recorded using a self-calibrating heat flux sensor (HFP01SC, Hukseflux, Delft, The Netherlands), an anemometer (A100R, Vector Instruments, Rhyl, U.K.), and a humidity probe (HMP45C, Vaisala, Helsinki, Finland) located above the canopy. Soil temperature and water content were measured using soil heat flux sensors (TCAV, Campbell Scientific, Logan, Utah) and water content reflectometers (CS616-L, Campbell Scientific) located near the surface and at depths of 20, 50, 100, 200, and 500 mm. A tipping-bucket raingauge (TE525MM, Campbell Scientific) was located 70 cm above the ground.

Radiation exchange was collected using a four-component net radiometer (CNR-1, Kipp and Zonen, Delft, The Netherlands), which includes two pyranometers (0.3 to 3 µm) for incoming and reflected solar radiation measurement (S_d and S_u) and two pyrgeometers (5 to 50 µm) for downward and upward infrared measurement (L_d and L_u); net all-wave radiation (R_n) was calculated from the four components using equation 1. The four separate sensors were calibrated to equal sensitivity.

Model simulations were validated using (1) measured upward and downward long-wave radiation (L_u and L_d), (2) upward short-wave radiation (S_u), and (3) net all-wave radiation (R_n), from 15 June to 28 October (days 166 to 301) in 2003. Maximum plant height of maize was about 2.60 m with a leaf area index of 5.58. Model results were evaluated using model efficiency (ME; Nash and Sutcliffe, 1970), mean bias error (MBE), and root mean square deviation (RMSD; Flerchinger et al., 2003). Model efficiency is analogous to coefficient of determination, with the exception that ME ranges from negative infinity to 1.0; negative ME values indicate that the mean observation is a better predictor than simulated values. Definitions of model performance measures are listed in table 1.

Table 1. Descriptions and definitions of model performance measures.

Measure	Description	Mathematical Definition[a]
ME	Model efficiency, i.e., variation in measured values accounted for by the model	$1-\frac{\sum_{i=1}^{N}\left(Y_i-\hat{Y}_i\right)^2}{\sum_{i=1}^{N}\left(Y_i-\bar{Y}\right)^2}$
RMSD	Root mean square difference between simulated and observed values	$\left[\frac{1}{N}\sum_{i=1}^{N}\left(\hat{Y}_i-Y_i\right)^2\right]^{1/2}$
MBE	Mean bias error of model predictions compared to observed values	$\frac{1}{N}\sum_{i=1}^{N}\left(\hat{Y}_i-Y_i\right)$

[a] $\hat{Y}_i$ = simulated values, Y_i = observed values, $\bar{Y}$ = mean of observed values, and N = the number of observations.

Model Description

The SHAW model consists of a vertical, one-dimensional profile extending downward from the vegetation canopy, snow, residue, or soil surface to a specified depth within the soil. A layered system is established through the plant canopy, snow, residue, and soil, and each layer is represented by an individual node. Version 2.3 of the SHAW model, referred to as SHAW23, was used for this study. Additionally, two separate modifications were made to the model to improve the long-wave radiation exchange. The first modification, referred to as SHAW-Ld, employs the best method from a variety of tested algorithms for estimating downward long-wave radiation at the field site. The second modification, referred to as SHAW-TLC, uses canopy leaf temperature rather than canopy air temperature to compute long-wave emittance by the plant canopy layers. The following subsections describe the three versions of the model.

SHAW23 Model

Detailed descriptions of energy and mass transfer calculations within the canopy and residue layers were given by Flerchinger and Pierson (1991), Flerchinger et al. (1998), and Flerchinger and Saxton (1989). Short- and long-wave radiation exchange between canopy layers, residue layers, and the snow or soil surface are computed by considering downward direct radiation and upward and downward diffuse radiation being transmitted, reflected, and adsorbed by each layer. The upward flux of diffuse short-wave radiation between canopy layers i and i+1 ($S_{u,i}$) is computed as:

$$S_{u,i}=\tau_{d,i}S_{u,i+1}+\alpha(1-\tau_{d,i+1})S_{d,i}+\alpha(1-\tau_{b,i+1})S_{b,i} \quad (2)$$

where $\tau_{d,i}$ is the transmissivity of canopy layer i to diffuse radiation, $\tau_{b,i}$ is the transmissivity of canopy layer i to direct (or beam) radiation, α is the albedo of the canopy leaves, and

$S_{d,i}$ and $S_{b,i}$ are diffuse and direct radiation entering canopy layer i+1. A similar expression can be written for downward radiation at any point in the canopy. The SHAW model can simulate a multi-species canopy, and the transmissivity to direct radiation for each canopy layer is calculated from:

$$\tau_{b,i} = \exp\left(\sum_{j=1}^{NP} K_j L_{i,j}\right) \tag{3}$$

where $L_{i,j}$ and K_j are leaf area index and extinction coefficient, respectively, for plant species j of canopy layer i, and NP is the number of plant species. Assuming a spherical leaf orientation for the maize canopy of the current study, the extinction coefficient for direct radiation was computed from (Campbell, 1977):

$$K = \frac{1}{2\sin\beta} \tag{4}$$

where β is the solar angle with the local slope. An approximate expression for diffuse transmissivity using an extinction coefficient of 0.7815 was employed (error less than 0.03 for total leaf area index less than 8).

Transmission and absorption of long-wave radiation are similar to those of short-wave radiation, with the exception that there is no direct radiation and long-wave emittance must be considered. For simplicity, long-wave emittance of a canopy layer is calculated using a leaf temperature for all plant species that is equal to air temperature within the layer and is therefore biased by the difference between canopy air temperature and leaf temperature.

Typically, long-wave parameterizations use screen-level temperature and humidity information to calculate clear-sky fluxes. The SHAW model uses the Stefan-Boltzmann equation to estimate clear-sky downward long-wave radiation:

$$L_{clr} = \varepsilon_{clr}\sigma T_o^{\,4} \tag{5}$$

where T_o is screen-level air temperature (K), and σ is the Stefan-Boltzmann constant. Clear-sky emissivity (ε_{clr}) is computed from the relation given by Idso and Jackson (1969):

$$\varepsilon_{clr} = 1 - 0.261e^{-0.00077T^2} \tag{6}$$

where T is screen-level air temperature (°C). Clear-sky emissivity is adjusted for cloudy situations by an empirical cloud cover correction, which depends on the total cloudiness (Unsworth and Monteith, 1975):

$$\varepsilon_a(c) = (1 - 0.84c)\varepsilon_{clr} + 0.84c \tag{7}$$

Here, ε_a is atmospheric emissivity adjusted for cloud cover, and c is the mean daily fraction of cloud cover, which ranges from 0 to 1. Cloudiness is estimated from a daily clearness index (k), which is defined as the ratio of daily solar radiation flux density to total hemispherical solar radiation flux density incident on a horizontal surface at the outer edge of the earth's atmosphere. Cloud cover is assumed to vary linearly from clear skies for $k > 0.6$ to complete cloud cover for $k < 0.35$.

SHAW-Ld Model

Several algorithms have been developed to estimate downward surface long-wave radiation flux using synoptic observations only. We assessed seven algorithms for estimating clear-sky downwelling long-wave flux (L_{clr}) for our field site. Five of these are of the same form as equation 5 and compute ε_{clr} as a function of screen-level water-vapor pressure (e_o) and air temperature (T_o) or as a function of e_o alone. In this article, the unit of the radiative flux is W m^{-2}, the unit of e_o is kPa, and the unit of T_o is K. A detailed explanation of the following forms for estimating L_{clr} is presented by Niemelä et al. (2001):

Ångström (1918):

$$L_{clr} = (A - B\times 10^{-0.067e_o})\sigma T_o^{\,4} \tag{8}$$

Brunt (1932):

$$L_{clr} = (A + B\sqrt{e_o})\sigma T_o^{\,4} \tag{9}$$

Brutsaert (1975):

$$L_{clr} = \left[A\left(\frac{e_o}{T_o}\right)^{1/7}\right]\sigma T_o^{\,4} \tag{10}$$

Idso (1981):

$$L_{clr} = \left[A + Be_o\exp\left(\frac{1500}{T_o}\right)\right]\sigma T_o^{\,4} \tag{11}$$

Prata (1996):

$$L_{clr} = \left[1 - (1+w)\exp\left(-[A+Bw]^{1/2}\right)\right]\sigma T_o^{\,4} \tag{12}$$

Swinbank (1963):

$$L_{clr} = A + BT_o^{\,6} \tag{13}$$

Dilley and O'Brien (1998):

$$L_{clr} = A + B\left(\frac{T_o}{273.16}\right)^6 + C\sqrt{w/2.5} \tag{14}$$

where A, B, and C are empirical coefficients, and w is the precipitable water (cm). Clear-sky long-wave radiation computed from the equations 8 through 14 must be adjusted for cloud cover. Two approaches for accounting for cloud cover are presented by Jacobs (1978) and Maykut and Church (1973):

Jacobs (1978):

$$L_d = (E + Fc)\times L_{clr} \tag{15}$$

Maykut and Church (1973):

$$L_d = (E + Fc^{2.75})\times L_{clr} \tag{16}$$

where E and F are empirical coefficients, and c is fraction of cloud cover. The best algorithms for estimating L_{clr} were selected and combined with these two methods along with that from Unsworth and Monteith (1975) in equation 7, as discussed subsequently in the Results and Discussion. Four additional schemes for directly estimating downward long-wave radiation of variably cloudy skies introduced by Aubinet (1994) were also evaluated:

Table 2. ME, RMSD, and MBE of algorithms simulating L_{clr} for clear days during 2003 (days 157, 167, 175, 223, 253, 254, 287-291, 293-296, and 299-301) using coefficients reported in the literature (mean of observed L_{clr} is 302.1 W m^{-2}).

Algorithm	Coefficients *A*	*B*	*C*	ME	RMSD (W m^{-2})	MBE (W m^{-2})
Ångströn (1918)	0.83	0.18	n/a	0.58	30.3	15.7
Brunt (1932)	0.52	0.205	n/a	0.76	22.7	−6.2
Brutsaert (1975)	1.723	n/a	n/a	0.74	23.6	8.6
Idso (1981)	0.70	5.95e−4	n/a	0.47	33.8	26.9
Prata (1966)	1.20	3.0	n/a	0.68	26.5	13.0
Swinbank (1963)	0.0	5.31e−13	n/a	0.33	38.2	15.5
Dilley and O'Brien (1998)	59.38	113.7	96.96	0.79	21.0	2.0

Table 3. ME, RMSD, and MBE of algorithms simulating L_d for all days (days 153 through 301) using coefficients reported in the literature (mean of observed L_d is 381.3 W m^{-2}).

Algorithm	Coefficients *A*	*B*	*C*	*D*	ME	RMSD (W m^{-2})	MBE (W m^{-2})
$L(T_o, k)$	−29	1.01	−19.9	n/a	0.71	26.4	−6.2
$L(T_o, e_o, k)$	181.0	12.6	−13	0.341	0.83	20.1	−6.8
$L(e_o, k)$	276.3	17.7	−9.93	n/a	0.76	24.1	−11.3
$L(e_o)$	0.925	0.0352	0.133	n/a	0.79	22.7	−3.4
Brunt and Unsworth	0.51	0.23	n/a	n/a	0.76	23.9	7.7
Brutsaert and Unsworth	1.20	n/a	n/a	n/a	0.72	26.0	14.3
Dilley and Unsworth	59.38	113.7	96.96	n/a	0.79	22.7	8.0

$L_d(T_o, k)$:

$$L_d = \sigma(-A + BT_o - Ck)^4 \tag{17}$$

$L_d(T_o, e_o, k)$:

$$L_d = \sigma(A + B\ln e_o - Ck + DT_o)^4 \tag{18}$$

$L_d(e_o, k)$:

$$L_d = \sigma(A + B\ln e_o - Ck)^4 \tag{19}$$

$L_d(e_o)$:

$$L_d = (A + B\ln e_o + C\ln[1-k])\sigma T_o^4 \tag{20}$$

where k is a daily clearness index defined above.

SHAW-TLC Model

The original SHAW23 model uses canopy air temperature rather than leaf temperature to compute long-wave emittance by the plant as a simplification of the canopy and leaf energy balance for each layer. In this study, the SHAW-TLC model avoids this simplification by computing long-wave emittance using canopy leaf temperature. The changes required to accomplish this were rather straightforward for the current application because it involves only a single plant species. Therefore, long-wave radiation transfer between different plant species with differing leaf temperatures within a canopy layer was not an issue for the current study. The mathematics for transfer between canopy elements within a canopy layer have not been worked out and are beyond the scope of this study. However, before this modification is permanently implemented into the model, radiation transfer between different plant species occupying the same canopy layer will need to be addressed.

Results and Discussion

Algorithm Selection for the SHAW-Ld Model

The algorithms for L_{clr} in equations 8 through 14 were used to calculate downward long-wave radiation using the data for clear days (days 157, 167, 175, 223, 253, 254, 287-291, 293-296, and 299-301, with a daily clearness index greater than 0.6). Coefficients reported by Niemelä et al. (2001) and the resulting goodness-of-fit measures are given in table 2. The algorithms by Brunt (1932), Brutsaert (1975), and Dilley and O'Brien (1998) yielded the best estimates, with ME ranging from 0.74 to 0.79. For perspective, ME for equation 6 was 0.29 for this same period.

The three best algorithms for clear-sky conditions were combined with equation 7 to account for cloud cover and compared with equations 17 through 20 using all data from days 153 through 301. Because Dilley and O'Brien's formulation does not compute ε_{clr} directly, an effective ε_{clr} was computed based on the predicted L_{clr} and used in equation 7. Results presented in table 3 indicate that the formulation of $L_d(T_o, e_o, k)$ from Aubinet (1994) performed the best, with ME equaling 0.83. This presents a substantial improvement over the original SHAW model formulation, which had an ME of 0.63 for this same period.

In order to better simulate L_d for the site, regressions were performed to obtain the optimum coefficients for equations 8 through 20. Therefore, regressions of L_{clr} for equations 8 through 14 were performed using the same clear days in 2003. The resulting coefficients and performance measures are presented in table 4. The ME of the algorithms from Idso (1981) and Dilley and O'Brien (1998) were 0.83 and 0.84, respectively, significantly higher than the others (table 4). The RMSD and MBE for these algorithms were less than the others as well; Dilley and O'Brien's MBE even reached zero. Therefore, these two algorithms for clear-sky radiation were combined with schemes by Jacobs (1978) and Maykut and Church (1973), which account for cloud cover. Regressions using all of the available downward long-wave radiation data resulted in the coefficients presented in table 5 for downward long-wave radiation of variably cloudy skies for our field site. (Results of combining the clear-sky formulations of Idso (1981) or Dilley and O'Brien (1998) with equation 7 to account for cloud cover were no better than those presented in table 5.) The formulation of $L_d(T_o, e_o, k)$ was best, with the

Table 4. ME, RMSD, and MBE of algorithms simulating L_{clr} using best-fit coefficients for clear days during 2003 (days 157, 167, 175, 223, 253, 254, 287-291, 293-296, and 299-301) (mean of observed L_{clr} is 302.1 W m^{-2}).

Algorithm	Coefficients *A*	*B*	*C*	ME	RMSD (W m^{-2})	MBE (W m^{-2})
Ångströn (1918)	1.45	0.84	n/a	0.78	22.1	1.0
Brunt (1932)	0.51	0.23	n/a	0.78	22.0	0.9
Brutsaert (1975)	1.20	n/a	n/a	0.78	21.8	−1.4
Idso (1981)	0.60	7.87e−4	n/a	0.83	19.3	0.5
Prata (1966)	0.25	3.17	n/a	0.79	21.4	−0.9
Swinbank (1963)	78.19	3.75e−13	n/a	0.56	31.5	0.0
Dilley and O'Brien (1998)	42.32	89.74	156.6	0.84	18.6	0.0

Table 5. ME, RMSD, and MBE of algorithms simulating L_d for all days (days 153 through 301) using best-fit coefficients (mean of observed L_d is 381.3 W m^{-2}).

Algorithm0	Coefficients *A*	*B*	*C*	*D*	*E*	*F*	ME	RMSD (W m^{-2})	MBE (W m^{-2})
$L(T_o, k)$	−12.0	1.05	−27.4	n/a	n/a	n/a	0.74	24.9	−0.8
$L(T_o, e_o, k)$	137.09	12.83	−16.8	0.50	n/a	n/a	0.88	17.7	2.7
$L(e_o, k)$	278.8	18.56	−12.72	n/a	n/a	n/a	0.82	21.0	−0.5
$L(e_o)$	0.920	0.07	0.16	n/a	n/a	n/a	0.82	20.6	0.5
Idso and Unsworth	0.60	7.87e−4	n/a	n/a	n/a	n/a	0.70	26.8	15.9
Idso and Jacobs	0.60	7.87e−4	n/a	n/a	0.99	0.08	0.72	25.9	2.2
Dilleyand Jacobs	42.32	89.74	156.6	0.84	1.0	0.10	0.82	20.9	1.0
Idso and Maykut	0.60	7.87e−4	n/a	n/a	1.0	0.07	0.73	25.4	2.1
Dilley and Maykut	42.32	89.74	156.6	0.84	1.02	0.08	0.82	20.7	0.8

Table 6. ME, RMSD, and MBE of schemes simulating L_d from days 1 to 305 in 2004 using best-fit coefficients from 2003 (mean of observed L_d is 330.42 W m^{-2}).

	ME	RMSD (W m^{-2})	MBE (W m^{-2})
$L(T_o, k)$	0.82	30.1	8.5
$L(T_o, e_o, k)$	0.91	22.0	−3.4
$L(e_o, k)$	0.88	25.0	−2.5
$L(e_o)$	0.90	22.6	−0.6
Idso and Jacobs	0.84	28.8	−6.6
Dilley and Jacobs	0.88	25.0	−5.8
Idso and Maykut	0.84	28.7	−5.9
Dilley and Maykut	0.88	24.9	−4.8

highest ME (0.88) and lowest RMSD (17.68 W m^{-2}). Although this algorithm had the largest MBE, 2.7 W m^{-2} is rather insignificant. An F-test comparing the RMSD for $L_d(T_o, e_o, k)$ using the original coefficients (table 3) and the regressed coefficients (table 6) indicated that the regressed coefficients were a significant improvement ($p < 0.001$).

Before selecting an algorithm for L_d to incorporate into the SHAW model, each of the proposed equations was validated using data collected during 2004. Model performance measures for the algorithms applied to the 2004 data are presented in table 6. Again, the best algorithm was $L_d(T_o, e_o, k)$ with ME of 0.91, RMSD of 22.0 W m^{-2}, and MBE of 2.53 W m^{-2}. Thus, the expression for $L_d(T_o, e_o, k)$ given in equation 16 with coefficients presented in table 5 was selected and incorporated as a modification in the SHAW-Ld model as the best method to compute downward long-wave radiation at the top of the canopy for the field site.

Model Validation

The three versions of the SHAW model were initialized on day 166 (15 June) and allowed to simulate downward and upward long-wave radiation (L_d, L_u) and upward short-wave radiation (S_u) as well as net all-wave radiation (R_n) through day 301 (28 October). Simulated and measured values were compared using model efficiency (ME), mean bias error (MBE), and root mean square deviation (RMSD).

Comparisons of measured and simulated results are as shown in table 7 and figures 1 to 3 for the three models. S_u and R_n were simulated well by all of the models, with ME values of 0.97 or greater, while the RMSD for R_n of SHAW-Ld was lower than the others due to the improvement in long-wave radiation simulation. Of the four components, the long-wave radiation was simulated the poorest by all three models. Downward long-wave radiation and upward long-wave radiation are similar in magnitude (table 7) and tend to cancel each other, but these fluxes are present the entire day, in contrast to solar radiation, and therefore require further attention.

Table 7. Comparison of measured and simulated hourly radiation from 15 June to 28 October (days 166 to 301) of 2003 for the three versions of the SHAW model.

	Average[a] (W m^{-2})	SHAW23 ME	SHAW23 RMSD (W m^{-2})	SHAW23 MBE (W m^{-2})	SHAW-TLC ME	SHAW-TLC RMSD (W m^{-2})	SHAW-TLC MBE (W m^{-2})	SHAW-Ld ME	SHAW-Ld RMSD (W m^{-2})	SHAW-Ld MBE (W m^{-2})
R_n	80.9	0.98	26.0	2.9	0.98	26.0	2.9	0.98	22.6	−4.7
L_d	382.1	0.68	28.6	12.1	0.68	28.6	12.1	0.88	17.7	2.7
L_u	428.9	0.89	15.1	8.3	0.87	16.3	8.4	0.91	13.8	6.5
S_u	26.3	0.97	7.3	1.5	0.97	7.3	1.5	0.97	7.3	1.5

[a] Average is the mean of hourly measured radiation from 15 June to 28 October (days 166 to 301).

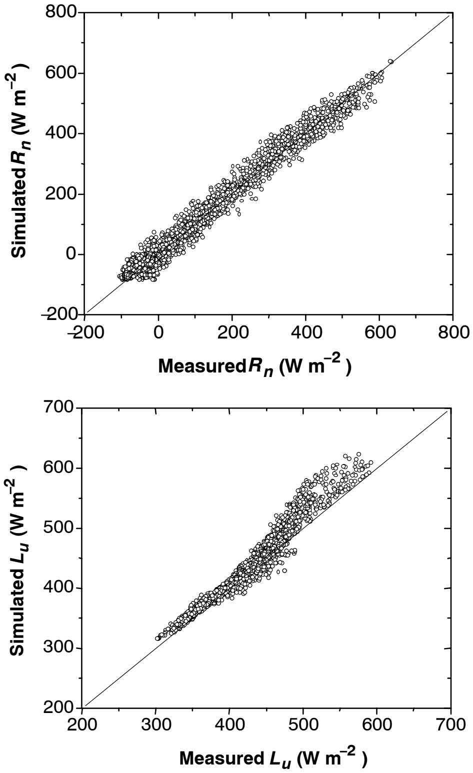

Figure 1. Hourly R_n, L_d, L_u, and S_u simulated by SHAW23 versus measurement from 15 June to 28 October (days 166 to 301) of 2003. (All fluxes are in W m^{-2}).

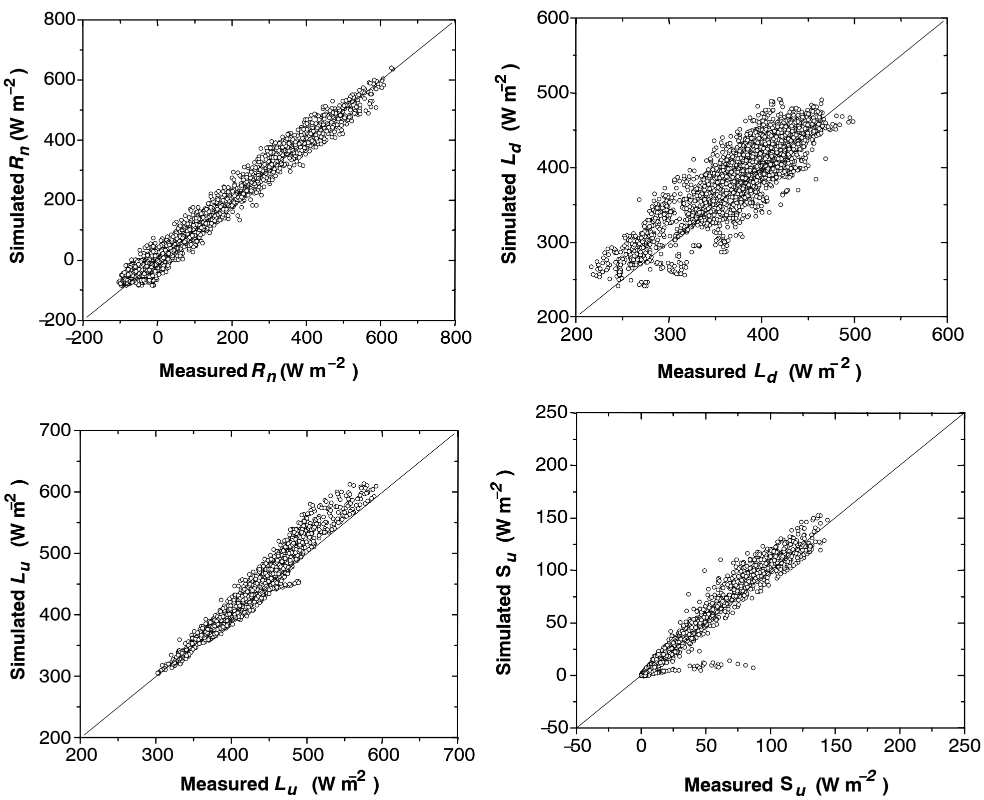

Figure 2. As shown in figure 1 but for SHAW-TLC.

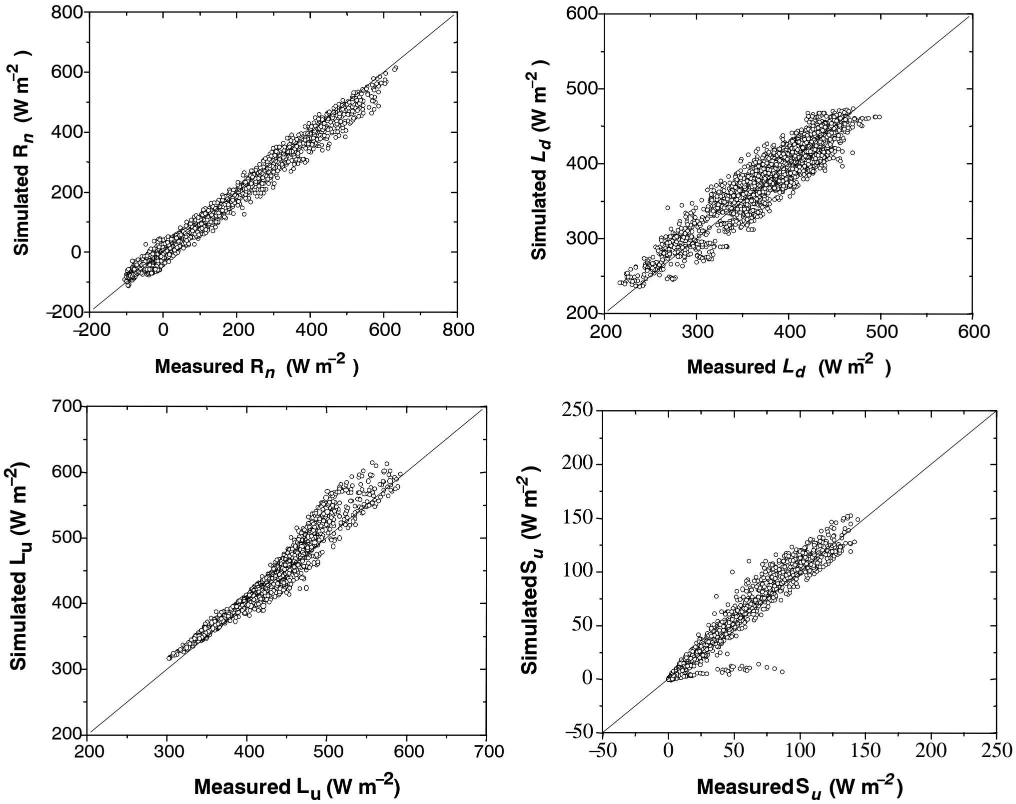

Figure 3. As shown in figure 1 but for SHAW-Ld.

The SHAW-Ld version of the model resulted in improved prediction of the L_d values, with ME rising from 0.68 to 0.88. This translated to a slight improvement in L_u as well, with ME increasing from 0.89 to 0.91 (table 7). Correspondingly, bias between simulated and measured values reduced as MBE fell from 12.13 to 2.73 W m^{-2} for L_d, and from 8.29 to 6.52 W m^{-2} for L_u. Unfortunately, SHAW-TLC, which should better represent long-wave radiation flux within the canopy, did not improve the prediction of L_u, with ME falling from 0.89 to 0.87.

To assess the diurnal performance for long-wave radiation simulation of the models, hourly performance statistics are presented for L_d of SHAW23 and SHAW-Ld in table 8, for L_u of the three models in table 9, and for all radiation components on a single clear day in figure 4. Undoubtedly, SHAW-Ld improved the simulation of L_d at each hour, with increased ME and reduced RMSD (table 8). The plots in figure 4 show that although the models overestimated midday values, they followed the general trend of L_d slightly increasing around midday for day 225. The sudden fluctuation in measured L_d around hours 3 to 7 and hours 21 to 24 illustrates the difficulty in accurately simulating L_d, as these changes are likely due to changes in cloud cover; the algorithms for L_d do not account for diurnal changes in cloud cover. The MBE in table 8 indicates that on average SHAW23 underestimated L_d from midnight to morning, and overestimated it at other times. It is still not clear why the poorest simulation of both models appeared in the evening, as indicated in table 8 by the higher RMSD values during the evening hours.

All of the models performed well in simulating L_u during nighttime hours, with ME greater than 0.90 and RMSD less during the night than for daytime hours (table 9). However, L_u was consistently overestimated for all hours except by SHAW-TLC for some morning hours. This trend is consistent with the hourly variation plotted for day 225 in figure 4. The largest bias for all models was found around noon. This consistent overestimation of L_u explains why SHAW-TLC did not improve the simulation, especially during the daytime. Leaf temperature used by SHAW-TLC was normally higher than canopy air temperature during the day at this site and lower at night. Thus, using leaf temperature to compute emitted long-wave radiation exacerbated the overestimation of L_u during the day, but improved the bias error during nighttime hours. One might speculate that the overprediction of canopy and leaf temperature was due to errors in simulating the latent cooling of the canopy; however, Xiao et al. (2006) show that the model actually overpredicted evapotranspiration during this period.

It may be postulated that the overprediction of L_u may be attributed to the K-theory used in the models. Wilson et al. (2003) found that the main difference between K-theory and Lagrangian theory was in simulation of radiometric temperature, since K-theory consistently predicted higher canopy radiometric temperatures than L-theory by 2°C to 8°C, depending on leaf area index. Indeed, Xiao et al. (2006) showed that SHAW tends to overpredict canopy leaf temperature, particularly around noon.

Conclusions

The objectives of this research were to: (1) validate all-wave radiation components simulated by the SHAW model over the canopy surface, i.e., long-wave (including

Table 8. Comparison of measured and simulated downward long-wave radiation for each hour of the day from 15 June to 28 October (days 166 to 301) of 2003 for the original SHAW23 model and the modified SHAW-Ld model.

Hour	Average[a] (W m^{-2})	SHAW23 ME	SHAW23 RMSD (W m^{-2})	SHAW23 MBE (W m^{-2})	SHAW-Ld ME	SHAW-Ld RMSD (W m^{-2})	SHAW-Ld MBE (W m^{-2})
1:00	376.86	0.77	23.4	−1.1	0.88	17.0	−0.6
2:00	377.18	0.77	22.8	−2.2	0.86	18.0	−0.7
3:00	378.19	0.76	23.2	−5.1	0.85	18.0	−2.9
4:00	378.06	0.76	23.5	−6.6	0.85	18.3	−4
5:00	378.80	0.75	24.1	−8.3	0.85	18.7	−5.4
6:00	379.14	0.75	24.8	−8.1	0.85	19.5	−5.3
7:00	380.81	0.74	26.5	−4.6	0.84	21.2	−2.8
8:00	379.87	0.79	24.9	5.8	0.87	19.7	4.1
9:00	380.17	0.77	26.3	15.6	0.89	18.5	8.0
10:00	385.10	0.71	28.1	19.2	0.9	16.4	5.7
11:00	389.37	0.67	28.9	21.8	0.93	13.2	3.0
12:00	393.57	0.64	29.6	22.5	0.94	11.9	−0.1
13:00	395.89	0.61	31.1	23.8	0.94	11.7	−1.7
14:00	396.42	0.55	33.1	25.8	0.94	12.4	−2.2
15:00	394.07	0.47	36.1	28.5	0.93	13.1	−0.8
16:00	389.23	0.4	39.0	32.2	0.91	14.9	3.8
17:00	384.46	0.39	40.0	32.6	0.86	19.0	8.5
18:00	379.53	0.49	37.3	29.2	0.82	21.9	12.6
19:00	376.18	0.63	31.5	22.8	0.82	22.0	13.2
20:00	374.70	0.72	26.9	17.0	0.84	20.5	11.5
21:00	374.77	0.76	24.6	12.6	0.85	19.5	8.9
22:00	375.63	0.76	24.0	8.5	0.85	19	5.9
23:00	375.89	0.78	22. 5	5.5	0.87	17.3	4.2
0:00	376.37	0.8	21.4	2.8	0.89	16.2	2.4

[a] Average is the mean of hourly measured radiation from 15 June to 28 October (days 166 to 301).

Table 9. Comparison of measured and simulated upward long-wave radiation in each hour from 15 June to 28 October (days 166 to 301) of 2003.

Hour	Average[a] (W m^{-2})	SHAW23 ME	SHAW23 RMSD (W m^{-2})	SHAW23 MBE (W m^{-2})	SHAW-TLC ME	SHAW-TLC RMSD (W m^{-2})	SHAW-TLC MBE (W m^{-2})	SHAW-Ld ME	SHAW-Ld RMSD (W m^{-2})	SHAW-Ld MBE (W m^{-2})
1:00	405.47	0.95	7.3	4.5	0.96	6.8	0.2	0.95	7.2	3.8
2:00	404.05	0.95	7.1	4.1	0.95	7.0	0.2	0.96	6.9	3.7
3:00	402.86	0.96	6.8	3.7	0.95	7.1	−0.3	0.96	6.6	3.6
4:00	401.52	0.96	6.9	3.7	0.95	7.1	−0.2	0.96	6.6	3.8
5:00	401.19	0.96	7.0	3.9	0.95	7.4	−0.1	0.96	6.5	4.0
6:00	403.69	0.96	7.4	5.4	0.96	7.0	2.3	0.96	7.2	5.6
7:00	412.39	0.93	9.6	7.5	0.93	9.8	7.2	0.94	9.1	7.2
8:00	425.75	0.87	12.7	8.9	0.81	15.6	12.7	0.89	11.6	8.2
9:00	440.39	0.8	16.1	9.5	0.68	20.4	16.6	0.84	14.6	8.3
10:00	452.89	0.72	20.4	10.7	0.56	25.2	20.2	0.76	18.7	9.0
11:00	462.60	0.63	24.7	12.2	0.49	29.0	23.0	0.68	22.8	10.1
12:00	468.41	0.62	26.8	13.1	0.54	29.4	22.9	0.67	24.8	10.5
13:00	470.96	0.63	26.9	13.3	0.59	28.7	21.9	0.69	24.8	10.5
14:00	469.47	0.69	24.7	12.8	0.63	26.8	19.4	0.74	22.4	9.7
15:00	463.89	0.76	21.0	12.0	0.73	22.3	15.3	0.82	18.2	8.5
16:00	455.76	0.83	17.1	11.0	0.83	17.1	10.0	0.88	14.3	7.4
17:00	445.01	0.87	14.5	10.3	0.88	13.9	5.8	0.91	12.1	6.7
18:00	432.54	0.9	12.7	10.7	0.93	10.9	6.2	0.93	10.8	7.2
19:00	421.92	0.91	11	9.5	0.95	8.3	5.4	0.93	9.4	6.0
20:00	415.46	0.92	9.5	7.9	0.96	7.3	3.9	0.93	8.9	5.0
21:00	412.31	0.93	8.8	6.8	0.96	7.0	2. 8	0.93	8.7	4.6
22:00	409.89	0.94	8.4	6.2	0.96	7.1	2.2	0.94	8.5	4.4
23:00	408.00	0.94	8.1	5.7	0.96	7.0	1.7	0.94	8.3	4.4
0:00	406.45	0.95	7.6	5.2	0.96	6.8	1.2	0.95	7.8	4.2

[a] Average is the mean of hourly measured radiation from 15 June to 28 October (days 166 to 301).

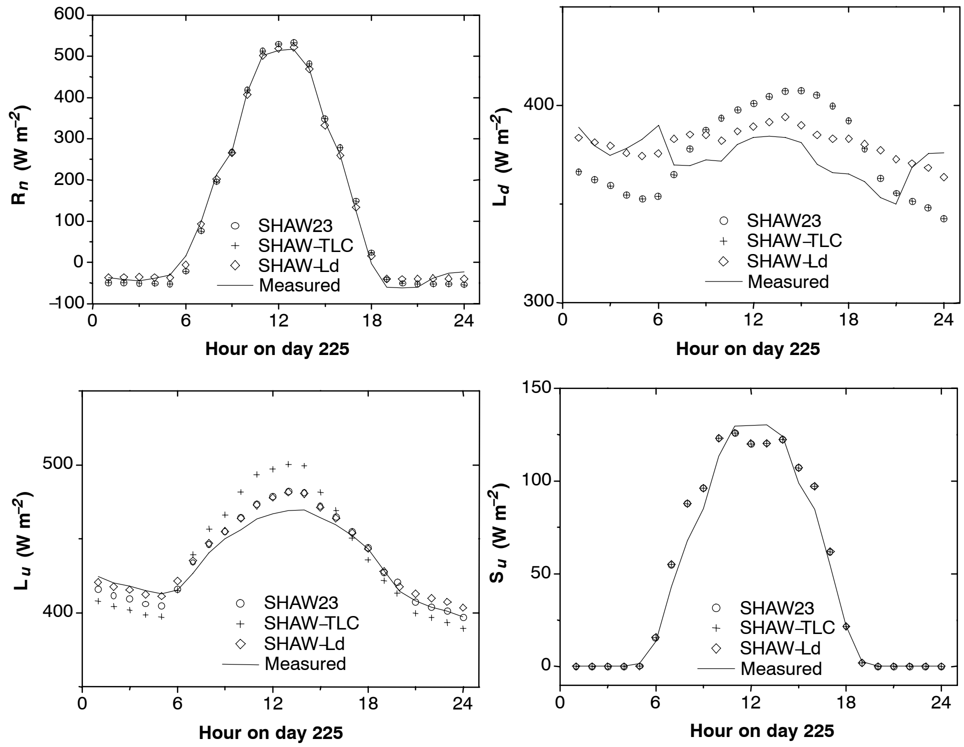

Figure 4. R_n, L_d, L_u**, and** S_u **simulated by SHAW23, SHAW-TLC, and SHAW-Ld versus measurement at each hour on 13 August (day 225) of 2003. (All fluxes are in W m**$^{-2}$**).**

down and upward) and short-wave radiation (including down and upward); and (2) evaluate modifications to improve simulation of the surface radiation exchange. Version 2.3 of the SHAW model (SHAW23) was run with data from 15 June to 29 October of 2003 collected in Yucheng, China. Two modified versions of the model to improve simulated long-wave radiation transfer were developed and tested. All simulations were validated with measurements from the field site. The SHAW-TLC model calculated long-wave emittance using leaf temperature instead of canopy air temperature, and SHAW-Ld calculated L_d using a published empirical algorithm, calibrated and validated with data from the site. The results indicated that the SHAW23 model did not predict long-wave radiation as well as net all-wave and short-wave radiation, and SHAW-TLC did not improve the prediction of L_u. However, SHAW-Ld improved the simulation of L_d and L_u considerably.

The main limitation of using the algorithm for calculating downward sky long-wave radiation lies in the choice of appropriate values for cloud cover and cloud type. The formulae are statistical correlations of radiation fluxes with weather variables at particular sites and do not describe direct functional relationships. For prediction, they are most accurate under average conditions, e.g., when the air temperature does not increase or decrease rapidly with height near the surface and when the air is not unusually dry or humid. They are therefore appropriate for climatological studies of radiation balance but are often not accurate enough for micrometeorological analyses over periods of a few hours. In particular, the equations cannot be used to investigate the diurnal variation of L_d.

All three models overpredicted L_u most of the time. Because SHAW23 uses canopy air temperature, which is typically cooler than leaf temperature during midday at this field site, the bias in L_u was reduced compared to SHAW-TLC, i.e., using canopy air temperature in SHAW23 tended to compensate for the overprediction in leaf temperatures. However, bias in nighttime values of L_u was lowest for SHAW-TLC. While the SHAW model simulates the radiation balance and transfer processes within the canopy reasonably well, these results demonstrate some areas for model improvement. Specifically, overprediction of midday canopy temperatures should be corrected before implementing the SHAW-TLC modifications.

Acknowledgements

This work is supported by National Natural Science Foundation of China (Grant No. 40328001).

References

Ångströn, A. 1918. A study of the radiation of the atmosphere. *Smithsonian Misc. Collect.* 65: 1-159.

Aubinet, M. 1994. Longwave sky radiation parametrizations. *Solar Energy* 53(2): 147-154.

Brunt, D. 1932. Notes on radiation in the atmosphere. *Quarterly J. Royal Meteor. Soc.* 58(247): 389-420.

Brutsaert, W. 1975. On a derivable formula for long-wave radiation from clear skies. *Water Resources Res.* 11(5): 742-744.

Campbell, G. S. 1977. *An Introduction to Environmental Biophysics.* New York, N.Y.: Springer-Verlag.

Dilley, A. C., and D. M. O'Brien. 1998. Estimating downward clear sky long-wave irradiance at the surface from screen temperature and precipitable water. *Quarterly J. Royal Meteor. Soc.* 124(549): 1391-1401.

Duffin, E. K. 1999. Evaluating snowmelt runoff, infiltration, and erosion in a sagebrush-steppe ecosystem. MS thesis. Utah. Logan, Utah: Utah State University, Watershed Science Program.

Flerchinger, G. N., and C. L. Hanson. 1989. Modeling soil freezing and thawing on a rangeland water shed. *Trans. ASAE* 32(5): 1551-1554.

Flerchinger, G. N., and F. B. Pierson. 1991. Modeling plant canopy effects on variability of soil temperature and water. *Agric. Forest Meteor.* 56(3-4): 227-246.

Flerchinger, G. N., and K. E. Saxton. 1989. Simultaneous heat and water model of a freezing snow-residue-soil system: I. Theory and development. *Trans. ASAE.* 32(2): 573-578.

Flerchinger, G. N., and M. S. Seyfried. 1997. Modeling soil freezing and thawing and frozen soil runoff with the SHAW model. In *Proc. International Symposium on Physics, Chemistry, and Ecology of Seasonally Frozen Soils*, 537-543. CRREL Special Report 97-10. Hanover, N.H.: U.S. Army Cold Regions Research and Engineering Laboratory.

Flerchinger, G. N., K. R. Cooley, and Y. Deng. 1994. Impacts of spatially and temporally varying snowmelt on subsurface flow in a mountainous watershed: 1. Snowmelt simulation. *Hydrol. Sci. J.* 39(5): 507-520.

Flerchinger, G. N., J. M. Baker, and E. J. A. Spaans. 1996a. A test of the radiative energy balance of the SHAW model for snowcover. *Hydrol. Proc.* 10(10): 1359-1367.

Flerchinger, G. N., C. L. Hanson, and J. R. Wight. 1996b. Modeling of evapotranspiration and surface energy budgets across a watershed. *Water Resources Res.* 32(8): 2539-2548.

Flerchinger, G. N., W. P. Kustas, and M. A. Weltz. 1998. Simulating surface energy fluxes and radiometric surface temperatures for two arid vegetation communities using the SHAW model. *J. Applied Meteor.* 37(5): 449-460.

Flerchinger, G. N., T. J. Sauer, and R. A. Aiken. 2003. Effects of crop residue cover and architecture on heat and water transfer at the soil surface. *Geoderma* 116(1-2): 217-233.

Hayhoe, H. N. 1994. Field testing of simulated soil freezing and thawing by the SHAW model. *Canadian Agric. Eng.* 36(4): 279-285.

Huntingford, C., S. J. Allen, and R. J. Harding. 1995. An intercomparison of single and dual-source vegetation-atmosphere transfer models applied to transpiration from Sahelian savannah. *Boundary-Layer Meteor.* 74(4): 397-418.

Hymer, D. C., M. S. Moran, and T. O. Keefer. 2000. Soil water evaluation using a hydrologic model and calibrated sensor network. *SSSA J.* 64(1): 319-326.

Idso, S. B. 1981. A set of equations for full spectrum and 8 to 14 μm and 10.5 to 12.5 μm thermal radiation from cloudless skies. *Water Resources Res.* 17(2): 295-304.

Idso, S. B., and R. D. Jackson. 1969. Thermal radiation from the atmosphere. *J. Geophys. Res.* 74(23): 5397-5403.

Jacobs, J. D. 1978. Radiation climate of Broughton Island. In *Energy Budget Studies in Relation to Fast-Ice Breakup Processes in Davis Strait* (Occas. Paper 26), 105-120. Boulder, Colo.: University of Colorado, Institute of Arctic and Alpine Research.

Kennedy, I., and B. Sharratt, B. 1998. Model comparisons to simulate frost depth. *Soil Sci.* 163(8): 636-645.

Maykut, G. A., and P. F. Church. 1973. Radiation climate of Barrow, Alaska, 1962-66. *J. Applied Meteor.* 12(4): 620-628.

Monteith, J. L. 1963. Gas exchange in plant communities. In *Environmental Control of Plant Growth*, 95-112. L. T. Evans, ed. New York, N.Y.: Springer.

Nash, J. E., and J. V. Sutcliffe. 1970. River flow forecasting through conceptual models: Part I. A discussion of principles. *J. Hydrol.* 10(3): 282-290.

Nassar, I. N., R. Horton, and G. N. Flerchinger. 2000. Simultaneous heat and mass transfer in soil columns exposed to freezing/thawing conditions. *Soil Sci.* 165(3): 208-216.

Niemelä, S., P. Räisänen, and H. Savijärvi. 2001. Comparison of surface radiative flux parameterizations: Part I. Longwave radiation. *Atmos. Res.* 58(1): 1-18.

Norman, J. M. 1979. Modeling the complete crop canopy. In *Modification of the Aerial Environment of Plants*, 249-277. B. J. Barfield and J. F. Gerber, eds. St. Joseph, Mich.: ASAE.

Prata, A. J. 1996. A new long-wave formula for estimating downward clear-sky radiation at the surface. *Quarterly J. Royal Meteor. Soc.* 122(533): 1127-1151.

Shuttleworth, W. J., and J. S. Wallace. 1985. Evaporation from sparse crops: An energy combination theory. *Quarterly J. Royal Meteor. Soc*. 111(469): 839-855.

Smith, J. A., and S. M. Goltz. 1994. A thermal exitance and energy balance model for forest canopies*. IEEE Trans. Geosci. Remote Sens*. 32(5): 1060-1066.

Swinbank, W. C. 1963. Long-wave radiation from clear skies. *Quarterly J. Royal Meteor. Soc.* 89(2): 339-348.

Unsworth, M. H., and J. L. Monteith. 1975. Long-wave radiation at the ground. *Quarterly J. Royal Meteor. Soc*. 101(427): 13-24.

Wilson T. B., J. M. Norman, W. L. Bland, and C. J. Kucharik. 2003. Evaluation of the importance of Lagrangian canopy turbulence formulations in a soil-plant-atmosphere model. *Agric. Forest Meteor.* 115(1-2): 51-69.

Xiao, W., Q. Yu, G. N. Flerchinger, and Y. F. Zheng. 2006. Evaluation of SHAW model in simulating energy balance, leaf temperature, and microclimate within a maize canopy. *Agron. J.* 98(3): 722-729.

Xu, X., J. L. Nieber, J. M. Baker, and D. E. Newcomb. 1991. Field testing of a model for water flow and heat transport in variably saturated, variably frozen soil. *Transportation Research Record* 1307: 300-308. Washington, D.C.: National Research Council, Transportation Research Board.

Zhao, W., and R. J. Qualls. 2005. A multiple-layer canopy scattering model to simulate shortwave radiation distribution within a homogeneous plant canopy. *Water Resources Res.* 41(8): W08409 (DOI: 10.1029/2005WR004016). 16 pp.